

Surface noise analysis using a single-ion sensor

N. Daniilidis,¹ S. Gerber,¹ G. Bolloten,¹ M. Ramm,¹ A. Ransford,¹ E. Ulin-Avila,¹ I. Talukdar,¹ and H. Häffner^{1,2,*}

¹Department of Physics, University of California, Berkeley, Berkeley, California 94720, USA

²Materials Sciences Division, Lawrence Berkeley National Laboratory, Berkeley, California 94720, USA

(Received 1 July 2013; revised manuscript received 21 May 2014; published 20 June 2014)

We use a single-ion electric-field noise sensor in combination with *in situ* surface treatment and analysis tools, to investigate the relationship between electric-field noise from metal surfaces in vacuum and the composition of the surface. These experiments are performed in a setup that integrates ion trapping capabilities with surface analysis tools. We find that treatment of an aluminum-copper surface with energetic argon ions significantly reduces the level of room-temperature electric-field noise, but the surface does not need to be atomically clean to show noise levels comparable to those of the best cryogenic traps. The noise levels after treatment are low enough to allow fault-tolerant trapped-ion quantum information processing on a microfabricated surface trap at room temperature.

DOI: 10.1103/PhysRevB.89.245435

PACS number(s): 37.10.Ty, 07.07.Df, 73.50.Td, 81.65.Cf

I. INTRODUCTION

Electric-field noise and the associated energy dissipation near surfaces and interfaces present challenges in many fields of science and technology. This includes modern nanoelectronics [1,2], superconducting electronics [3], studies of noncontact friction [4], microtraps for ions [5] and ultracold atoms [6], detection of Casimir forces [7], and tests of general relativity [8,9]. It is, therefore, imperative to gain a better understanding of the sources of such noise, so that appropriate solutions can be adopted.

In particular, electric-field noise near the electrode surfaces of ion traps has been known to cause unexpectedly high heating of the motional modes of laser-cooled, trapped ions [10]. The ion motion serves as a bus for quantum information in multi-ion quantum gates, and thus the noise has been a major impediment in efforts to realize trapped-ion based quantum information processors [11]. Such applications require the use of quantum error correction [12,13] which makes heating rates of the ion motion below 10 quanta/s desirable [11]. In addition, nascent efforts to realize hybrid quantum systems, where single atoms or ions can exchange quantum information with solid-state quantum devices [14–17], require minimizing the amount of electric-field noise from surfaces of metals in vacuum [18].

As a result of the technological importance of the electric-field noise from surfaces, there are significant ongoing efforts to understand and eliminate it. The noise has strong temperature dependence [19,20] and shows a $f^{-\alpha}$ frequency spectrum with typical values of α close to 1 [5,19,21–24]. Recently, the noise level near aluminum-copper surfaces was reduced after *in situ* pulsed-laser treatment [23]. A more significant reduction in the noise near a gold surface was achieved after argon plasma sputter treatment of a trap surface in vacuum, and analysis of an identical surface revealed that the treatment removed carbon contamination [5]. The latter work suggests a strong influence of carbon contaminants on the noise, but the actual mechanisms are not yet understood. Promising models for the noise exist [10,21,25–27], but experimental input is

necessary for the models to be further refined and adapted to the complexity of surfaces found in typical experiments.

While the noise reduction in [5] is a major advance toward scalable trapped-ion based quantum computing, such work also shows that trapped ions can serve as ultrasensitive detectors of certain surface properties. Detectors operating in the quantum regime can offer unparalleled levels of sensitivity [28]. Such systems can be used to measure weak forces [29,30], magnetic fields [31], and charges [32]. In the case of trapped ions, experimentalists have achieved extremely accurate control in preparing and measuring the ion quantum state [11]. Thus, by measuring the effect of electric-field noise on the motional quantum state of the ion, one can probe the noise in the frequency range from 100 kHz to a few MHz with remarkable sensitivity [10,30]. Such studies will ideally be performed in combination with other surface-characterization and modification tools to provide complementary information about the surface.

Here we combine a single-ion noise sensor in the same apparatus with surface analysis tools. We use single $^{40}\text{Ca}^+$ trapped ions to measure electric-field noise near the aluminum-copper electrodes of an ion trap, sputter treat the electrode surfaces using an Ar^+ ion beam, and correlate the noise spectra with the surface composition determined using *in situ* Auger spectroscopy. After Ar^+ treatment, the heating rate for the motional state of a $^{40}\text{Ca}^+$ ion trapped at 950 kHz is 3.8(0.5) quanta/s, low enough to allow fault-tolerant quantum information processing. We find that the carbon and oxygen levels of the treated surface increase on waiting in ultrahigh vacuum but the noise level does not, and thus surfaces do not need to be atomically clean or oxide free to show such low noise levels.

The paper is structured as follows: in Sec. II we describe the setup in which these experiments were performed and the fabrication procedure for the ion trap we used. We then present, in Sec. III, experimental results from the different tools in our setup, and we discuss our findings in Sec. IV.

Our experiments proceeded in the following way: after installing the trap in a vacuum, we baked the vacuum system and used a single ion to measure electric-field noise near the trap surface. We then analyzed the chemical composition of the surface *in situ*, sputter treated the trap surface, and analyzed

*hhaeffner@berkeley.edu

the chemical composition and electric-field noise near the trap surface at various stages after the initial treatment.

II. EXPERIMENTAL SYSTEM

A. Trapping apparatus

We performed the experiments in a multifunction vacuum system consisting of a 12-in. spherical chamber, which allows surface treatment, characterization, and ion trap operation, without breaking the vacuum (see Fig. 1). A microfabricated ion trap is mounted on a manipulator and can be rotated around the z axis. Depending on the trap orientation, the trap chip is facing an objective with numerical aperture ≈ 0.3 for ion fluorescence collection ($+y$ direction), an Ar^+ ion gun (45° with respect to the y axis), or an Auger/low-energy electron-diffraction (LEED) unit ($-y$ direction, OCI microengineering, BLD-8000), which allows us to characterize the elemental composition of the trap surface. A residual gas analyzer (RGA, ExTorr XT100M) is installed in the same chamber, with its axis at 45° with respect to y on the yz plane and allows us to analyze the residual gases in the chamber.

The static voltages for trapping are generated by low-noise digital-to-analog converters (AD660). To reduce electronic

noise injected to the trap electrodes, we filter the static voltage signals using sixth-order low-pass filters with insertion loss higher than 90 dB in the frequency range between 200 kHz and 1 MHz. The last filtering stage resides inside the vacuum and consists of 47-nF (AVX, X7R dielectric) capacitors on a printed circuit board (made of Rogers 4350), which supports the trap chip carrier, as well as 0.68-nF (AVX, X7S dielectric) capacitors, which are wire-bonded on the chip carrier. The wirebonds attached to the electrodes of our trap contribute an Ohmic resistance of approximately $5\ \Omega$ to the impedance connected between our trap electrodes and the ground. We estimate the real part of the in-vacuum filtering capacitor impedance to be $0.1\ \Omega$ at 1 MHz and the real part of the impedance of filtering capacitors outside our vacuum system to be $0.8\ \Omega$ at 1 MHz.

The entire vacuum system, including the electronics for the radio-frequency and static trapping potentials, can be housed inside a Faraday cage providing more than 40 dB of attenuation for electromagnetic fields in the range of frequencies between 200 kHz and 1 MHz, in which we have performed electric-field noise measurements. As mentioned in the introduction, and elaborated in Sec. III, we used single ions to measure electric-field noise near the trap surface. We measured the electric-field noise without the Faraday cage prior to sputter treatment of the surface and measured noise both with and without the cage after treatment. This allowed us to estimate the technical (i.e., non-surface-related) noise level in the absence of the Faraday cage to be between 2% (at 200 kHz) and 20% (at 1 MHz) of the total electric-field noise prior to treatment.

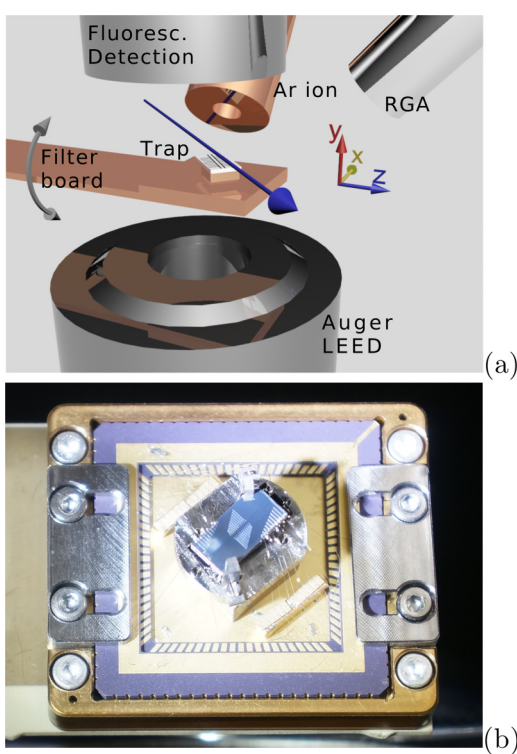


FIG. 1. (Color online) (a) The vacuum system, integrating a surface trap (center) attached to a filter board (yellow, left), mounted on a 360° rotational holder (rotation about the z axis), an Auger and low-energy electron-diffraction spectrometer (bottom), an Ar^+ gun (behind the xy plane), an observation channel (above), and a residual gas analyzer (RGA, upper right). The laser direction (blue arrow) is at a 7° angle with the trap axis [oriented along $(-1,0,1)$], defined by the radio-frequency trap electrodes (black lines on the trap). For clarity, the center of the coordinate system is offset with respect to the trapping position. (b) Photograph of the mounted trap.

B. Trap fabrication

In this work, we used a microfabricated surface electrode trap, trapping ions at a distance of $100\ \mu\text{m}$ from the nearest electrode. The trap consists of a fused quartz chip on which the electrode pattern was etched using a combination of pulsed-laser weakening and hydrofluoric acid etching (performed by Translume, Ann Arbor, MI) [33]. The design of the trap chip is shown in Fig. 2. The gaps between electrodes are approximately $10\ \mu\text{m}$ wide and $50\ \mu\text{m}$ deep. After the substrate was etched, we cleaned it in Piranha solution at 120°C and evaporated a metal film combination of 15-nm Ti, 500-nm Al, 30-nm Cu, 15-nm Ti, 500-nm Al, and 30-nm Cu, in an electron beam evaporator with vacuum better than 3×10^{-6} torr, without allowing the aluminum surfaces to oxidize in air before the copper layer evaporation. The copper layers serve the purpose of preventing oxidation of the aluminum surfaces while the evaporator vacuum is broken between the two aluminum layer evaporation.

Subsequently, we mounted the trap on a chip carrier without allowing it to come into contact with any solvents. The chip is mechanically held onto a Kyocera 84 pin ceramic leadless chip carrier (CLCC). The CLCC is mounted onto the in-vacuum filter board using a socket constructed from Vespel and makes electrical contact with the filter board using Fuzz Button® pins. After assembly we baked the vacuum system with the trap at 160°C for three weeks, to achieve vacuum close to 2×10^{-10} torr (3×10^{-8} Pa). Between the electron beam evaporation and the vacuum bake, the chip was exposed to air for close to 72 h.

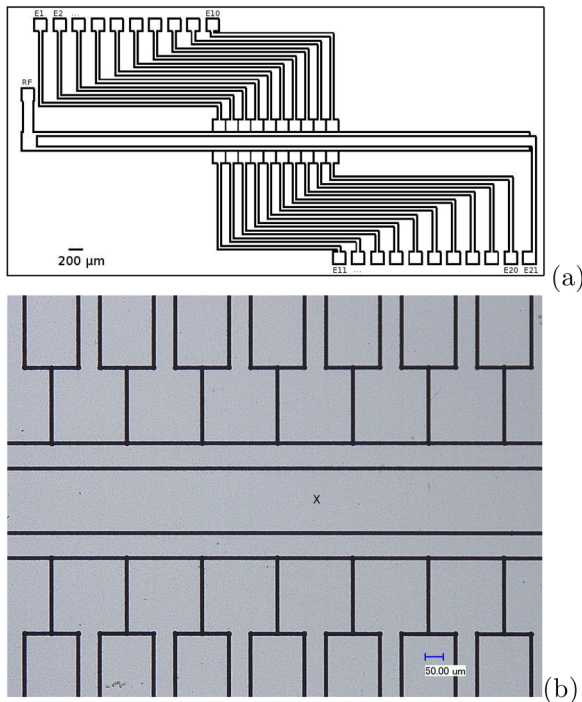


FIG. 2. (Color online) The trap used in this work. (a) Schematic of the trap electrodes. The surface trap has two long, symmetric electrode rails along the trap axis for rf confinement (RF) and 21 electrodes used for the static confinement (E1–E21). The rf electrode can also be biased at a static potential. In the experiments described here, ions were trapped near the center of the trap (at the center of electrodes E5 and E15). The electrodes are wire bonded using 25- μm -diameter Pd wire at the pads near the periphery of the chip. (b) Optical microscope image of the trapping region. Electrodes E1 to E8 and E11 to E18 are shown. The trapping position, next to electrodes E5 and E15, is marked by an “x.”

We trapped single ions along the trap axis, at the position defined by the line connecting the centers of electrodes E5 and E15 (see Fig. 2). Typical trap frequencies were between 200 kHz and 1 MHz in the axial direction and approximately 2.5 and 3.5 MHz in the radial directions, respectively. Ion heating rates, and thus the electric-field noise, were only measured along the axial direction, as we discuss in Sec. III.

III. EXPERIMENTAL RESULTS

After baking, we used single ions to measure the electric-field noise of the trap and performed surface analysis using the Auger spectrometer. Following this, we treated the trap surface using an Ar^+ beam and reanalyzed the surface. We then used a single ion to measure the noise spectrum after a 40-day waiting period and recorded Auger spectra from the surface within a few days from the noise measurement. Finally, we repeated the Ar^+ surface treatment, noise measurement, and Auger analysis steps one more time, all within a few days of each other. We performed both Ar^+ treatment runs under the same conditions. The argon pressure was 10^{-4} torr, the ion beam energy was 300 eV, the angle of incidence was perpendicular to the trap surface, and the beam flux was $2 \times 10^{17} \text{ m}^{-2} \text{ s}^{-1}$. We carried

out each treatment step for a total of 20 min, resulting in an estimated removal of 10 nm of material from the surface.

A. Surface composition

In Fig. 3, we show the Auger spectra of the trap surface at various stages, taken with an incident electron energy of 2 keV. The electron beam generated by our Auger spectrometer has a diameter of approximately 4 mm, and consequently the spectra represent the average composition over such a diameter centered around the trapping region. The spectra were taken after carefully positioning the Auger electron beam to within 1 mm of the center of the trapping region. We identify aluminum, copper, carbon, and oxygen peaks on the Auger spectra of the trap after the vacuum bake. After treatment, we additionally identify traces of argon, entrapped on the trap surface; iridium, thorium and lutetium, a result of outgassing of the Auger spectrometer surfaces; and palladium, resulting from partial overlap of the Auger beam with the wirebonds.

After baking, both carbon and oxygen were present on the trap surface. After treatment, the carbon and oxygen KLL peaks (i.e., involving electronic transitions between K and L shells) [34,35] were reduced by approximately 90%, but their ratio remained unchanged [Figs. 3(b) and 3(c), label B]. In addition, the chemical shift of the $\text{Al}(LMM)$ peak indicates that the aluminum oxide was removed. After the wait period of 40 days, the carbon peak increased roughly by a factor of 2, whereas the oxygen peak increased by a factor of 5, and the aluminum partially oxidized [Figs. 3(b) and 3(c), label C]. Thus, in this period carbon compounds were readSORBED or diffused to the surface, and some oxidation of the trap surface took place. After the second Ar^+ treatment step, both carbon and oxygen peaks were reduced by a factor of 2, but a significant amount of oxygen remained [Figs. 3(b) and 3(c), label D].

We use the strengths of the copper MVV peak (involving transitions between the M shell and the valence band), aluminum and aluminum oxide LMM peak, carbon KLL peak, and oxygen KLL peak to quantify the elemental composition and surface coverage with carbon and oxygen. From the $\text{Cu}(MVV)$ and Al and $\text{Al}_2\text{O}_3(LMM)$ peaks, we determine that the surface atomic composition had almost equal amounts of copper and aluminum throughout our study. The comparison between aluminum and copper is straightforward, because the low-energy peaks do not rely on the sensitivity of our electron analyzer, which depends strongly on the electron energy, as seen in Fig. 3.

To quantitatively analyze the carbon and oxygen content, we have to correct for the difference in the energy-dependent sensitivity between the hemispherical retarding-field electron analyzer and cylindrical mirror analyzers for which Auger peak intensities are tabulated [34,35]. By rescaling the peak intensities by a factor proportional to the peak energy, E , as expected for a generic retarding-field analyzer [34], we obtain coverage between 0.01 and 0.1 monolayers of carbon and oxygen throughout our study. However, such a low level of coverage cannot explain the large increase in the aluminum and copper peaks after treatment, shown in Fig. 3(a) [34,36]. To circumvent this inconsistency, we need to take into account the low sensitivity of our analyzer at high energies, already noted

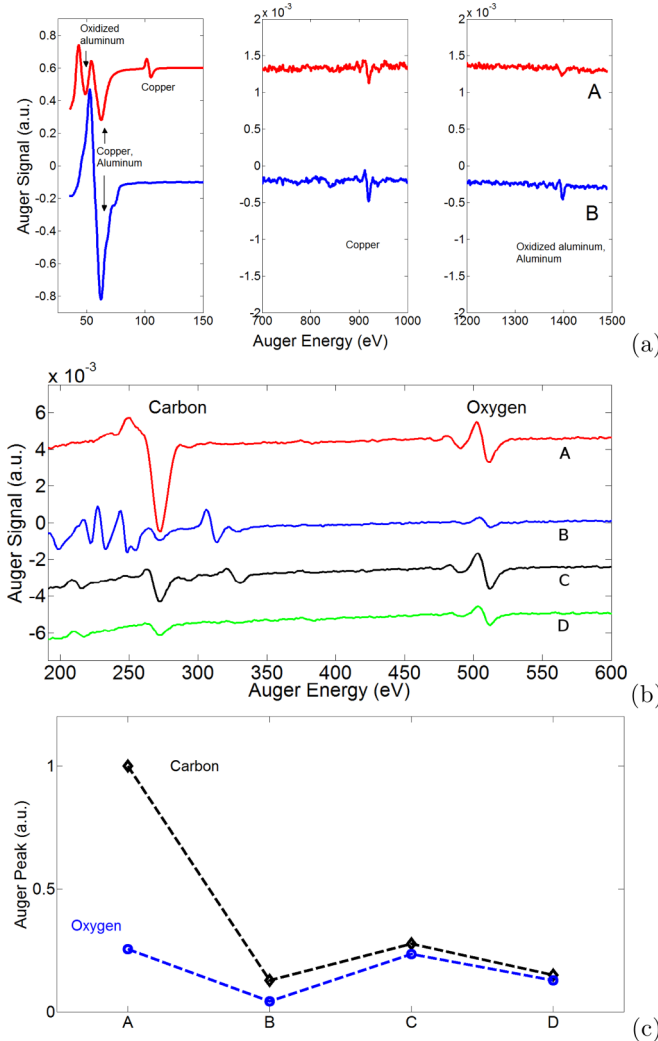


FIG. 3. (Color online) (a) Copper and aluminum peaks after the vacuum bake (A) and after Ar^+ sputter treatment (B). At low energies, the peaks corresponding to oxidized Al(LMM) and Cu(MVV) dominate (V represents valence-band electronic states). At higher energies, the Cu(LMM) and Al(KLL) peaks are three orders of magnitude weaker, due to poor sensitivity of the analyzer at high energies (note the expanded vertical axis). (b) Auger spectra showing the C(KLL) and O(KLL) peaks at different stages of surface treatments: after the bake (red, A), after the first treatment (blue, B), after 40 days in vacuum (black, C), and after the second treatment (green, D). In addition to carbon (270 eV) and oxygen (515 eV), traces of thorium and iridium (energies of 225, 245, and 255 eV) appear in B, a result of outgassing of the Auger filament. Lutetium (320 and 330 eV), possibly from the LEED fluorescent screen, is also visible in B. Traces of argon (200 and 215 eV) are visible in B, C, and D. A palladium peak, coming from the Pd wirebonds used, appears at 335 eV in C. The appearance of the palladium peak is a result of the large width of the Auger electron beam. Vertical axis units for all figures in (a) and (b) are the same. (c) Evolution of the signal strengths of oxygen (blue, circle) and carbon (black, diamond) in (b) normalized to the pretreatment carbon value.

in relation to the metal peak heights in Fig. 3(a). We achieve this by rescaling the peak intensities in the range from 50 to 600 eV by factors of the form $E/\text{eV} + 1.3 \times 10^{-6}(E/\text{eV})^4$. Such rescaling gives more self-consistent results for the

coverage and the variation of the metal peak heights. This analysis gives combined carbon and oxygen coverage of between 0.3 and 1.5 monolayers. Regardless of our choice for the energy sensitivity of the spectrometer, the carbon and oxygen coverage after the sputter-treated surface has been recontaminated is a sizable fraction of the pretreatment value, as is evident also from the peak heights in Fig. 3.

An RGA analysis of the residual gases in our vacuum system revealed that the predominant gases which can be responsible for the increase in the carbon and oxygen levels were carbon monoxide, at a pressure of approximately 8×10^{-11} torr (1×10^{-8} Pa), and water vapor at a pressure of 2.5×10^{-11} torr (3×10^{-9} Pa). These pressures correspond to exposure of the treated trap surface to approximately 280 L of CO and 80 L of H_2O , during the 40-day wait period between the spectra shown in Figs. 3(b) and 3(b) [37].

B. Electric-field noise

In parallel with these measurements, we used laser-cooled $^{40}\text{Ca}^+$ ions to determine the electric-field noise spectral density at a distance of $100 \mu\text{m}$ from the trap surface. Laser cooled ions have typical kinetic energies corresponding to temperature in the range of $10 \mu\text{K}$ to 1 mK , far below the equilibrium temperature of environmental noise sources. Thus, in the absence of laser cooling, cold ions heat up, with a heating rate determined by the electric-field noise spectral density at the ions' motion frequency [10]. By measuring the rate of change in the mean population of a particular mode of the ion motion, denoted here by $\dot{\bar{n}}$, the electric-field noise spectral density is given by $S_E = \frac{4m\hbar\omega}{e^2}\dot{\bar{n}}$, where m is the ion mass, ω is the frequency of the measured ion mode, and e is the elementary charge [10,21]. We measured heating rates by laser cooling the ion, waiting for a variable delay time, and determining the change in the average population, \bar{n} , of one particular mode of the ion motion. This method determines the noise spectral density for one particular component of the electric field, in our case the electric field along the trap axis [direction $\frac{1}{\sqrt{2}}(-1, 0, 1)$ in Fig. 1].

We used spectroscopy and resolved sideband cooling on the $S_{1/2}-D_{5/2}$ transition of the $^{40}\text{Ca}^+$ ion to determine the ion temperature, and thus the heating rate. Before the Ar^+ treatment of the trap surface, the high ion heating rates prevented us from sideband cooling to the motional ground state, and thus the heating rates were measured on ions cooled to the Doppler limit of the $S_{1/2}-P_{1/2}$ transition. Specifically, we determined the mean value of the thermal state of the ion motion by measuring the collapse of Rabi oscillations on the carrier and sideband transitions [10]. After surface treatment, the low noise of the trap allowed us to measure the heating rates on ions cooled to close to their ground state (average initial population \bar{n} of 0.2 quanta), by monitoring the relative strength of the red and blue sidebands of the $S_{1/2}-D_{5/2}$ transition [10]. We confirmed the consistency of these two methods by also measuring heating rates for Doppler-cooled ions for the trap after treatment.

Figure 4 shows the heating rates we obtained for the trap. Before Ar^+ treatment of the trap surface, we measured heating rates between 5000(1000) quanta/s and 200(10) quanta/s at motional frequencies between 246 and 852 kHz (red points).

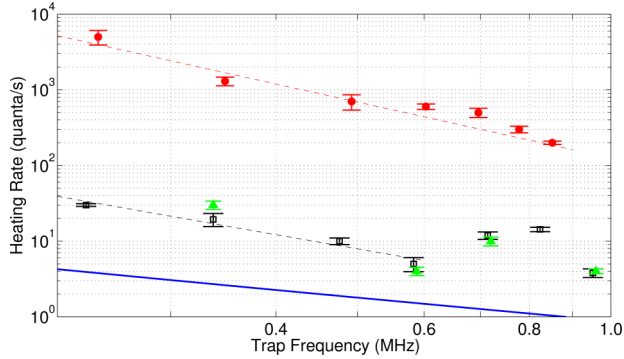


FIG. 4. (Color online) Frequency scaling of motional heating in our trap. Color coding for measured data is the same as in Fig. 3; i.e., red filled circles is pretreatment (A), black open squares is 40 days after Ar^+ treatment (C), and green filled triangles is after the second treatment (D). Dashed lines show fits of the form $\dot{n} \sim f^{-(1+\alpha)}$ (which corresponds to $S_E \sim f^{-\alpha}$). The extent of each line shows the range of frequencies over which the fit was performed. The solid line shows the expected Johnson noise heating for our setup.

The frequency scaling of these heating rates is $\dot{n} \sim f^{-2.27(0.23)}$, which implies a frequency scaling $S_E \sim f^{-1.27(0.23)}$ for the noise. As mentioned in Sec. II, a fraction between 2 and 20% of the noise before treatment was caused by external electromagnetic interference. This could result in underestimating the frequency scaling exponent, α , by as much as one σ . After treatment of the trap, we find much reduced heating rates between 30(1) and 3.8(0.5) quanta/s. The ion heating rates measured 2 days after treatment of the trap (green curve) are consistent with the values measured 40 days after treatment (black curve), despite the difference in carbon and oxygen content of the surface, seen in the Auger spectra. This shows that copper-aluminum surfaces do not need to be atomically clean and oxide free to achieve these low electric-field noise levels.

For the treated trap, we also observe a change of the spectral characteristics of the noise in the frequency range between 200 kHz and 1 MHz. The heating rates decrease with frequency between 200 and 580 kHz, and at higher frequencies they show a broad peak centered roughly around 800 kHz. The dropoff with frequency below 580 kHz has scaling $\dot{n} \sim f^{-1.95(0.28)}$, implying $S_E \sim f^{-0.95(0.28)}$. This scaling is consistent with what has been measured elsewhere [19,23]. However, the measured noise levels are close to the values expected from Johnson noise in our system, and we suspect that at this point we are limited by technical noise, rather than surface-related processes. We place a lower bound on the expected noise level of our setup by assuming the wirebonds and the capacitors in our setup display Johnson noise, with the real part of the impedance corresponding to $6\text{--}8 \Omega$ in the frequency range where we measured (blue line in Fig. 4). The peak at higher frequencies is reminiscent of resonant behavior and is consistent with a resonance in our filter board.

IV. DISCUSSION

It is instructive to compare the electric-field noise measured in this work with noise measured on other traps. To partially take into account the $f^{-\alpha}$ noise spectrum, it is customary to compare ωS_E for different traps. In Fig. 5 we

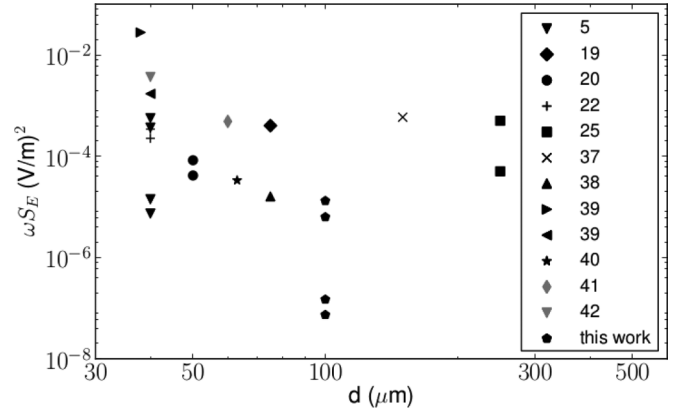


FIG. 5. Representative electric-field noise measurements for various ion traps with planar electrode geometries. All measurements were done at room temperature. Each symbol in the label corresponds to a different trap. For measurements where noise was reported over a range of frequencies, we show multiple data points, corresponding to the extreme frequency values.

summarize ωS_E versus the closest ion-electrode distance, for a number of trap noise measurements reported in the literature [5,19,20,22,25,38–43]. To compare between ion traps with different dimensions, one scales the noise with ion distance from the surface, d , as $S_E \sim d^{-4}$. This scaling is expected for noise arising from independently fluctuating, electrical-dipole-like sources on the surface [21]. Taking this type of scaling into account, our noise measurements prior to Ar^+ treatment fall below the general trend of room-temperature noise measurements.

In order to compare the noise near the treated aluminum-copper surface to the noise measured in a treated gold trap [5] we need to take into account the different frequencies, f , and ion-electrode distances, d . Such comparisons should be interpreted with caution, since the frequency and distance scaling of the noise are not well established. However, the expected range of scaling exponents provides a range of values on which to base the comparison. On the one extreme of the range, we assume a scaling $S_E \sim f^{-\alpha}d^{-4}$ with $\alpha = 1$ between 1.68 MHz and 950 kHz, and find that the noise on the Al-Cu surface is a factor of 2 lower than the noise on the Au surface, which lies within the range of day-to-day variations in noise measurements. If, on the other extreme, our post-treatment noise values are limited by technical noise, and the frequency scaling with exponent $\alpha \approx 1.5$ measured in [5] persists to 240 kHz, the noise from the aluminum-copper surface has to be a factor of 11 lower than the noise from the gold surface. The noise values we measured both before and after treatment suggest that aluminum and copper can be good candidates as trap fabrication materials.

In summary, we have probed the electric-field noise near an aluminum-copper surface at room temperature using a single trapped ion and performed *in situ* elemental analysis and treatment of the surface. We find that surface treatment leads to significant reduction in the noise level of the surface exposed to air and baked in a high vacuum, but the noise does not increase after the surface gets recontaminated in an ultrahigh vacuum. Thus, aluminum-copper surfaces do not need to be atomically clean or oxide free to show low noise

levels, comparable to those reported in [5]. These observations suggest that the noise level can depend strongly on coverage by surface contaminants, on the order of one monolayer.

ACKNOWLEDGMENTS

We would like to acknowledge M. Crommie for useful feedback and the loan of a LEED/AES spectrometer; D. Hite, D. Leibfried, G. Somorjai, E. Yablonovitch, and J. Bokor for

useful discussions; and P. Schindler for a critical reading of the manuscript. This research was funded by the Office of the Director of National Intelligence (ODNI), Intelligence Advanced Research Projects Activity (IARPA), through the Army Research Office Grant No. W911NF-10-1-0284. All statements of fact, opinion, or conclusions contained herein are those of the authors and should not be construed as representing the official views or policies of IARPA, the ODNI, or the US Government.

[1] E. Simoen, M. G. Caño de Andrade, M. Aoulaiche, N. Collaert, and C. Claeys, *IEEE Trans. Electron Devices* **59**, 1272 (2012).

[2] M. Ishigami, J. H. Chen, E. D. Williams, D. Tobias, Y. F. Chen, and M. S. Fuhrer, *Appl. Phys. Lett.* **88**, 203116 (2006).

[3] Yu. A. Pashkin, O. Astafiev, T. Yamamoto, Y. Nakamura, and J. S. Tsai, *Quant. Info. Proc.* **8**, 55 (2009).

[4] B. C. Stipe, H. J. Mamin, T. D. Stowe, T. W. Kenny, and D. Rugar, *Phys. Rev. Lett.* **87**, 096801 (2001).

[5] D. A. Hite, Y. Colombe, A. C. Wilson, K. R. Brown, U. Warring, R. Jördens, J. D. Jost, K. S. McKay, D. P. Pappas, D. Leibfried, and D. J. Wineland, *Phys. Rev. Lett.* **109**, 103001 (2012).

[6] C. Henkel, S. Pötting, and M. Wilkens, *Appl. Phys. B* **69**, 379 (1999).

[7] W. J. Kim, M. Brown-Hayes, D. A. R. Dalvit, J. H. Brownell, and R. Onofrio, *Phys. Rev. A* **78**, 020101(R) (2008); W. J. Kim, A. O. Sushkov, D. A. R. Dalvit, and S. K. Lamoreaux, *ibid.* **81**, 022505 (2010).

[8] S. E. Pollack, S. Schlamminger, and J. H. Gundlach, *Phys. Rev. Lett.* **101**, 071101 (2008).

[9] C. W. F. Everitt *et al.*, *Phys. Rev. Lett.* **106**, 221101 (2011).

[10] D. J. Wineland, C. Monroe, W. M. Itano, D. Leibfried, B. E. King, and D. M. Meekhof, *J. Res. Natl. Inst. Stand. Technol.* **103**, 259 (1998).

[11] H. Häffner, C. F. Roos, and R. Blatt, *Physics Reports* **469**, 155 (2008).

[12] J. Chiaverini, D. Leibfried, T. Schaetz, M. D. Barrett, R. B. Blakestad, J. Britton, W. M. Itano, J. D. Jost, E. Knill, C. Langer, R. Ozeri, and D. J. Wineland, *Nature (London)* **432**, 602 (2004).

[13] P. Schindler, J. T. Barreiro, T. Monz, V. Nebendahl, D. Nigg, M. Chwalla, M. Hennrich, and R. Blatt, *Science* **332**, 1059 (2011).

[14] L. Tian, P. Rabl, R. Blatt, and P. Zoller, *Phys. Rev. Lett.* **92**, 247902 (2004).

[15] A. André, D. DeMille, J. M. Doyle, M. D. Lukin, S. E. Maxwell, P. Rabl, R. J. Schoelkopf, and P. Zoller, *Nature Physics* **2**, 636 (2006).

[16] D. Kielpinski, D. Kafri, M. J. Woolley, G. J. Milburn, and J. M. Taylor, *Phys. Rev. Lett.* **108**, 130504 (2012).

[17] N. Daniilidis, D. J. Gorman, L. Tian, and H. Häffner, *New J. Phys.* **15**, 073017 (2013).

[18] N. Daniilidis and H. Häffner, *Annual Review of Condensed Matter Physics* **4**, 83 (2013).

[19] J. Labaziewicz, Y. Ge, D. R. Leibrandt, S. X. Wang, R. Shewmon, and I. L. Chuang, *Phys. Rev. Lett.* **101**, 180602 (2008).

[20] J. Chiaverini and J. M. Sage, *Phys. Rev. A* **89**, 012318 (2014).

[21] Q. A. Turchette, D. Kielpinski, B. E. King, D. Leibfried, D. M. Meekhof, C. J. Myatt, M. A. Rowe, C. A. Sackett, C. S. Wood, W. M. Itano, C. Monroe, and D. J. Wineland, *Phys. Rev. A* **61**, 063418 (2000).

[22] R. J. Epstein, S. Seidelin, D. Leibfried, J. H. Wesenberg, J. J. Bollinger, J. M. Amini, R. B. Blakestad, J. Britton, J. P. Home, W. M. Itano, J. D. Jost, E. Knill, C. Langer, R. Ozeri, N. Shiga, and D. J. Wineland, *Phys. Rev. A* **76**, 033411 (2007).

[23] D. T. C. Allcock, L. Guidoni, T. P. Harty, C. J. Ballance, M. G. Blain, A. M. Steane, and D. M. Lucas, *New J. Phys.* **13**, 123023 (2011).

[24] D. T. C. Allcock, T. P. Harty, H. A. Janacek, N. M. Linke, C. J. Ballance, A. M. Steane, D. M. Lucas, R. L. Jarecki, S. D. Habermehl, M. G. Blain, D. Stick, and D. L. Moehring, *Appl. Phys. B* **107**, 913 (2011).

[25] N. Daniilidis, S. Narayanan, S. Möller, R. Clark, T. Lee, P. Leek, A. Wallraff, St. Schulz, F. Schmidt-Kaler, and H. Häffner, *New J. Phys.* **13**, 013032 (2011).

[26] A. Safavi-Naini, P. Rabl, P. F. Weck, and H. R. Sadeghpour, *Phys. Rev. A* **84**, 023412 (2011).

[27] A. Safavi-Naini, E. Kim, P. F. Weck, P. Rabl, and H. R. Sadeghpour, *Phys. Rev. A* **87**, 023421 (2013).

[28] A. A. Clerk, M. H. Devoret, S. M. Girvin, F. Marquardt, and R. J. Schoelkopf, *Rev. Mod. Phys.* **82**, 1155 (2010).

[29] J. D. Teufel, T. Donner, M. A. Castellanos-Beltran, J. W. Harlow, and K. W. Lehnert, *Nature Nanotech.* **4**, 820 (2009).

[30] R. Maiwald, D. Leibfried, J. Britton, J. C. Bergquist, G. Leuchs, and D. J. Wineland, *Nature Physics* **5**, 551 (2009).

[31] D. Budker and M. Romalis, *Nature Physics* **3**, 227 (2007).

[32] M. H. Devoret and R. J. Schoelkopf, *Nature (London)* **406**, 1039 (2000).

[33] Y. Bellouard, A. Said, M. Dugan, and P. Bado, *Opt. Expr.* **12**, 2120 (2004).

[34] L. E. Davis, N. C. MacDonald, P. W. Palmberg, G. E. Riach, and R. E. Weber, *Handbook of Auger Electron Spectroscopy*, 2nd ed. (Perkin-Elmer, Eden Prairie, Minnesota, 1978).

[35] D. Briggs and M. P. Seah, *Practical Surface Analysis* (Wiley, New York, 1983).

[36] R. Memeo, F. Cicicacci, C. Mariani, and S. Ossicini, *Thin Solid Films* **109**, 159 (1983).

[37] The value of 1 L corresponds to gas exposure at a pressure of 10^{-6} torr for 1 s.

[38] D. T. C. Allcock, J. A. Sherman, D. N. Stacey, A. H. Burrell, M. J. Curtis, G. Imreh, N. M. Linke, D. J. Szwer, S. C. Webster, A. M. Steane, and D. M. Lucas, *New J. Phys.* **12**, 053026 (2010).

[39] D. T. C. Allcock, T. P. Harty, C. J. Ballance, B. C. Keitch, N. M. Linke, D. N. Stacey, and D. M. Lucas, *Appl. Phys. Lett.* **102**, 044103 (2013).

[40] J. M. Amini, H. Uys, J. H. Wesenberg, S. Seidelin, J. Britton, J. J. Bollinger, D. Leibfried, C. Ospelkaus, A. P. VanDevender, and D. J. Wineland, *New J. Phys.* **12**, 033031 (2010).

[41] S. Charles Doret, J. M. Amini, K. Wright, C. Volin, T. Killian, A. Ozakin, D. Denison, H. Hayden, C.-S. Pai, R. E. Slusher, and A. W. Harter, *New J. Phys.* **14**, 073012 (2012).

[42] D. R. Leibrandt, J. Labaziewicz, R. J. Clark, I. L. Chuang, R. J. Epstein, C. Ospelkaus, J. H. Wesenberg, J. H. Bollinger, D. Leibfried, David Wineland, D. Stick, J. Sterk, Christopher Monroe, C.-S. Pai, Y. Low, R. Frahm, and R. E. Slusher, *Quantum Inf. Comput.* **9**, 0901 (2009).

[43] S. Seidelin, J. Chiaverini, R. Reichle, J. J. Bollinger, D. Leibfried, J. Britton, J. H. Wesenberg, R. B. Blakestad, R. J. Epstein, D. B. Hume, W. M. Itano, J. D. Jost, C. Langer, R. Ozeri, N. Shiga, and D. J. Wineland, *Phys. Rev. Lett.* **96**, 253003 (2006).